



<b>Title</b>	A Class-F CMOS Oscillator
<b>Authors(s)</b>	Babaie, Masoud, Staszewski, Robert Bogdan
<b>Publication date</b>	2013-08-07
<b>Publication information</b>	Babaie, Masoud, and Robert Bogdan Staszewski. "A Class-F CMOS Oscillator." IEEE, August 7, 2013. <a href="https://doi.org/10.1109/JSSC.2013.2273823">https://doi.org/10.1109/JSSC.2013.2273823</a> .
<b>Publisher</b>	IEEE
<b>Item record/more information</b>	<a href="http://hdl.handle.net/10197/8419">http://hdl.handle.net/10197/8419</a>
<b>Publisher's statement</b>	© 2013 IEEE. Personal use of this material is permitted. Permission from IEEE must be obtained for all other uses, in any current or future media, including reprinting/republishing this material for advertising or promotional purposes, creating new collective works, for resale or redistribution to servers or lists, or reuse of any copyrighted component of this work in other works.
<b>Publisher's version (DOI)</b>	10.1109/JSSC.2013.2273823

Downloaded 2026-05-01 23:34:51

The UCD community has made this article openly available. Please share how this access benefits you. Your story matters! (@ucd\_oa)



© Some rights reserved. For more information

# A Class-F CMOS Oscillator

Masoud Babaie, *Student Member, IEEE*, and Robert Bogdan Staszewski, *Fellow, IEEE*

**Abstract**—An oscillator topology demonstrating an improved phase noise performance is proposed in this paper. It exploits the time-variant phase noise model with insights into the phase noise conversion mechanisms. The proposed oscillator is based on enforcing a pseudo-square voltage waveform around the LC tank by increasing the third-harmonic of the fundamental oscillation voltage through an additional impedance peak. This auxiliary impedance peak is realized by a transformer with moderately coupled resonating windings. As a result, the effective impulse sensitivity function (ISF) decreases thus reducing the oscillator's effective noise factor such that a significant improvement in the oscillator phase noise and power efficiency are achieved. A comprehensive study of circuit-to-phase-noise conversion mechanisms of different oscillators' structures shows the proposed class-F exhibits the lowest phase noise at the same tank's quality factor and supply voltage. The prototype of the class-F oscillator is implemented in TSMC 65-nm standard CMOS. It exhibits average phase noise of  $-136$  dBc/Hz at 3 MHz offset from the carrier over 5.9–7.6 GHz tuning range with figure-of-merit of 192 dBc/Hz. The oscillator occupies  $0.12$  mm<sup>2</sup> while drawing 12 mA from 1.25 V supply.

**Index Terms**—Class-F oscillator, impulse sensitivity function, phase noise, digitally controlled oscillator, VCO, transformer.

## I. INTRODUCTION

DESIGNING voltage-controlled and digitally-controlled oscillators (VCO, DCO) of high spectral purity and low power consumption is quite challenging, especially for GSM transmitter (TX), where the oscillator phase noise must be less than  $-162$  dBc/Hz at 20 MHz offset frequency from 915 MHz carrier [1]. At the same time, the RF oscillator consumes disproportionate amount of power of an RF frequency synthesizer [2], [3] and burns more than 30% of the cellular RX power [4], [5]. Consequently, any power reduction of RF oscillators will greatly benefit the overall transceiver power efficiency and ultimately the battery lifetime. This motivation has encouraged an intensive research to improve the power efficiency of an RF oscillator while satisfying the strict phase noise requirements of the cellular standards.

The traditional class-B oscillator (Fig. 1(a)) is the most prevalent architecture due its simplicity and robustness. However, its phase noise and power efficiency performance drops dramatically just by replacing the ideal current source with a real one. Indeed, the traditional oscillator reaches its best performance for the oscillation amplitude of near supply voltage  $V_{DD}$  [6], [7]. Therefore, the gm-devices  $M_{1/2}$  enter deep triode for part of the

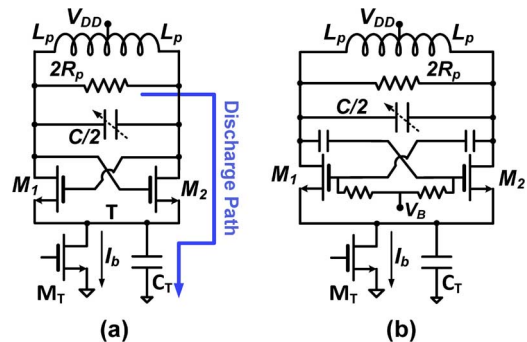


Fig. 1. Oscillator schematic: (a) traditional class-B; (b) class-C.

oscillation period. They exhibit a few tens of ohms of channel resistance. In addition, the tail capacitor  $C_T$  should be large enough to filter out thermal noise of  $M_T$  around the even harmonics of the fundamental, thus making a low impedance path between node “T” and ground. Consequently, the tank output nodes find a discharge path to the ground. It means that the equivalent Q-factor of the tank is degraded dramatically. This event happens alternatively between  $M_1$  and  $M_2$  transistors in each oscillation period. Hence, the phase noise improvement would be negligible by increasing the oscillation voltage swing when the gm-devices enter the triode region and thus, FoM drops dramatically. This degradation seems rather unavoidable in the simple structure of Fig. 1(a) since  $M_T$  must anyway be very large to reduce the  $1/f^3$  phase noise corner of the oscillator and thus its parasitic capacitor alone (i.e., even if  $C_T$  is zero) would be large enough to provide discharge path for the tank during the gm-device triode region operation.

The noise filtering technique [8] provides a relatively high impedance between the gm-devices and the current source. Hence, the structure maintains the intrinsic Q-factor of the tank during the entire oscillation period. However, it requires an extra resonator sensitive to parasitic capacitances, increasing the design complexity, area and cost.

Class-C oscillator (Fig. 1(b)), prevents the gm-devices from entering the triode region [9], [10]. Hence, the tank Q-factor is preserved throughout the oscillation period. The oscillator also benefits with 36% power saving from changing the drain current shape from square-wave of the traditional oscillator to the tall and narrow form for the class-C operation. However, the constraint of avoiding entering the triode region limits the maximum oscillation amplitude of the class-C oscillator to around  $V_{DD}/2$ , for the case of bias voltage  $V_B$  as low as a threshold voltage of the active devices. It translates to 6 and 3 dB phase noise and FoM penalty, respectively. Consequently, class-C voltage swing constraint limits the lowest achievable phase noise performance.

Harmonic tuning oscillator enforces a pseudo-square voltage waveform around the LC tank through increasing the third-harmonic component of the fundamental oscillation voltage

Manuscript received April 04, 2013; revised June 12, 2013; accepted July 11, 2013. Date of publication August 07, 2013; date of current version November 20, 2013. This paper was approved by Guest Editor Hooman Darabi. This work was supported in part by the European ERC Starting Grant 307624 TDRFSP.

The authors are with the Delft University of Technology, Delft, The Netherlands (e-mail: M.Masoud.Babaie@ieee.org; bogdans@ieee.org).

Color versions of one or more of the figures in this paper are available online at <http://ieeexplore.ieee.org>.

Digital Object Identifier 10.1109/JSSC.2013.2273823

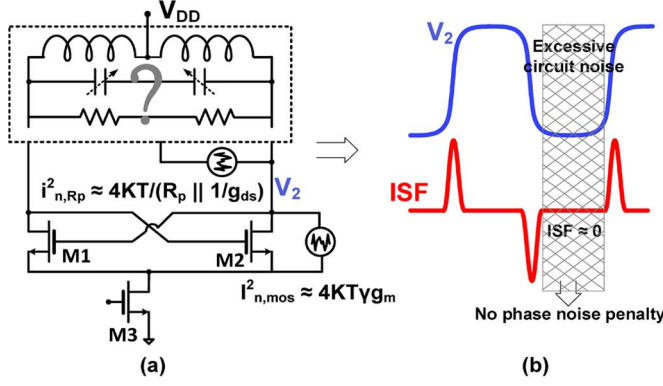


Fig. 2. Oscillator: (a) noise sources; (b) targeted oscillation voltage (top) and its expected ISF (bottom).

through an additional tank impedance peak at that frequency. Kim *et al.* [11] exploited this technique to improve the phase noise performance of the LC oscillator by increasing the oscillation zero-crossings slope. However, that structure requires more than two separate LC resonators to make the desired tank input impedance. It increases cost and decreases tuning range due to larger parasitics. Furthermore, the oscillator transconductance loop gain is the same for both resonant frequencies, thus raising the probability of undesired oscillation at the auxiliary tank input impedance. We have resolved the above mentioned concerns and quantified intuitively and theoretically the phase noise and power efficiency improvement of the class-F oscillator compared to other structures [12].

The paper is organized as follows. Section II establishes the environment to introduce the proposed class-F oscillator. The circuit-to-phase-noise conversion mechanisms are studied in Section III. Section IV presents extensive measurement results of the prototype, while Section V wraps up the paper with conclusions.

## II. EVOLUTION TOWARDS CLASS-F OSCILLATOR

Suppose the oscillation voltage around the tank was a square-wave instead of a sinusoidal. As a consequence, the oscillator would exploit the special ISF [13] properties of the square-wave oscillation voltage to achieve a better phase noise and power efficiency. However, the gm-devices would work in the triode region (shaded area in Fig. 2(b)) even longer than in case of the sinusoidal oscillator. Hence, the loaded resonator and gm-device inject more noise to the tank. Nevertheless, ISF value is expected to be negligible in this time span due to the zero derivative of the oscillation voltage [13]. Although the circuit injects huge amount of noise to the tank, the noise cannot change the phase of the oscillation voltage and thus there is no phase noise degradation.

### A. Realizing a Square-Wave Across the LC Tank

The above reasoning indicates that the square-wave oscillation voltage has special ISF properties that are beneficial for the oscillator phase noise performance. But how can a square-wave be realized across the tank? Let us take a closer look at the traditional oscillator in the frequency domain. As shown in Fig. 3, the drain current of a typical LC-tank oscillator is approximately a square-wave. Hence, it ideally has a fundamental and odd harmonic components. On the other hand, the tank input impedance

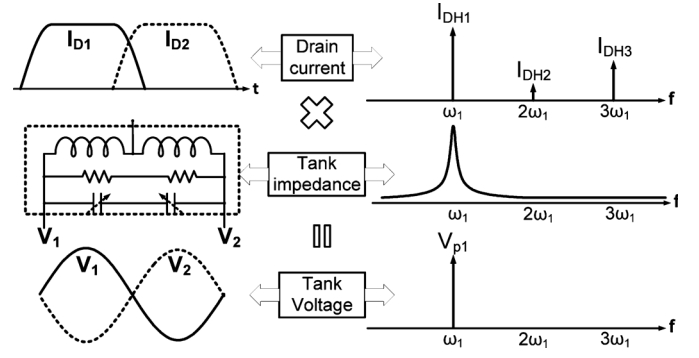


Fig. 3. Traditional oscillator waveforms in time and frequency domains.

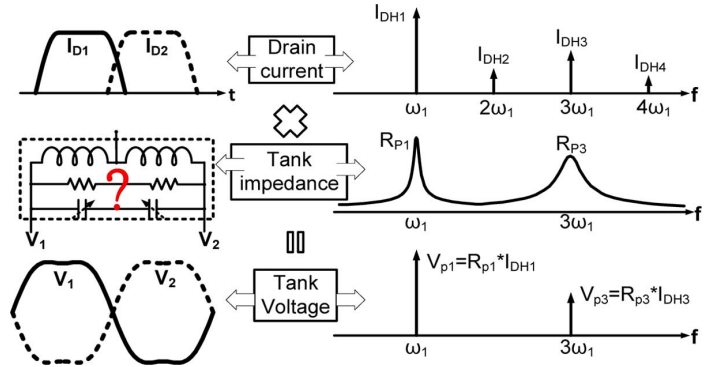


Fig. 4. Proposed oscillator waveforms in time and frequency domains.

has a magnitude peak only at the fundamental frequency. Therefore, the tank filters out the harmonic components of the drain current and finally a sinusoidal wave is seen across the tank.

Now, suppose the tank offers another input impedance magnitude peak around the third harmonic of the fundamental frequency (see Fig. 4). The tank would be prevented from filtering out the 3rd harmonic component of the drain current. Consequently, the oscillation voltage will contain a significant amount of the 3rd harmonic component in addition to the fundamental:

$$V_{in} = V_{p1} \sin(\omega_0 t) + V_{p3} \sin(3\omega_0 t + \Delta\phi) \quad (1)$$

$\zeta$  is defined as the magnitude ratio of the third-to-first harmonic components of the oscillation voltage.

$$\zeta = \frac{V_{p3}}{V_{p1}} = \left( \frac{R_{p3}}{R_{p1}} \right) \left( \frac{I_{DH3}}{I_{DH1}} \right) \approx 0.33 \left( \frac{R_{p3}}{R_{p1}} \right) \quad (2)$$

where,  $R_{p1}$  and  $R_{p3}$  are the tank impedance magnitudes at the main resonant frequency  $\omega_1$  and  $3\omega_1$ , respectively. Fig. 5 illustrates the oscillation voltage and its related expected ISF function (based on the closed-form equation in [13]) for different  $\zeta$  values. The ISF rms value of the proposed oscillation waveform can be estimated by the following expression for  $-\pi/8 < \Delta\phi < \pi/8$ .

$$\Gamma_{rms}^2 = \frac{1}{2} \frac{1 + 9\zeta^2}{(1 + 3\zeta)^2} \quad (3)$$

The waveform would become a sinusoidal for the extreme case of  $\zeta = 0, \infty$  so (3) predicts  $\Gamma_{rms}^2 = 1/2$ , which is well-known for the traditional oscillators.  $\Gamma_{rms}^2$  reaches its lowest value of  $1/4$  for  $\zeta = 1/3$ , translated to a 3 dB phase noise and

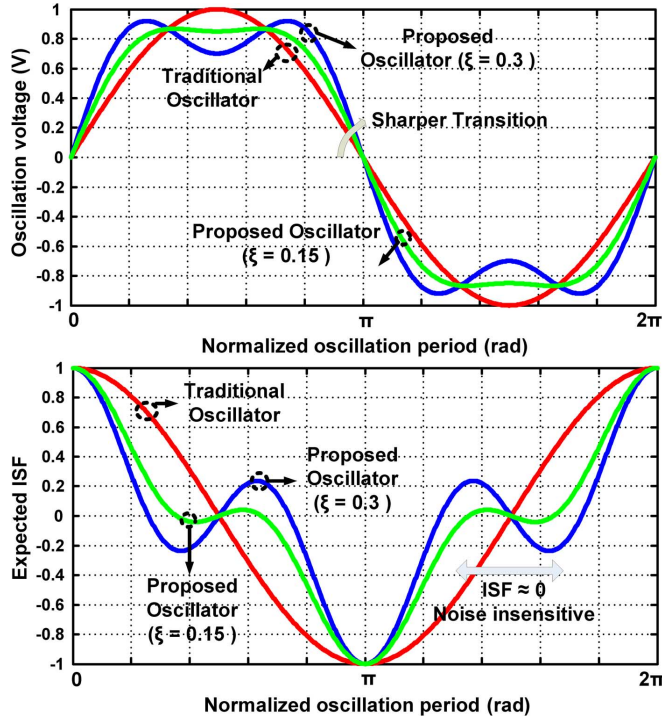


Fig. 5. The effect of adding 3rd harmonic in the oscillation waveform (top) and its expected ISF (bottom).

FoM improvement compared to the traditional oscillators. Furthermore, ISF of the proposed oscillator is negligible while the circuit injects significant amount of noise to the tank. Consequently, the oscillator FoM improvement could be larger than that predicted by just the ISF rms reduction.

### B. Proposed Tank

The argumentation related to Fig. 4 advocates the use of two resonant frequencies with a ratio of 3. The simplest way of realizing that would be with two separate inductors [11], [14]. However this will be bulky and inefficient. The chosen option in this work is a transformer-based resonator. The preferred resonator consists of a transformer with turns ratio  $n$  and tuning capacitors  $C_1$  and  $C_2$  at the transformer's primary and secondary windings, respectively (see Fig. 6). Equation (4), below, expresses the exact mathematical equation of the input impedance of the tank. where,  $k_m$  is the magnetic coupling factor of the transformer,  $r_p$  and  $r_s$  model the equivalent series resistance of the primary  $L_p$  and secondary  $L_s$  inductances [15]. The denominator of  $Z_{in}$  is a fourth-order polynomial for the imperfect coupling factor (i.e.,  $k_m < 1$ ). Hence, the tank contains two different conjugate pole pairs, which realize two different resonant frequencies. Consequently, the input impedance has two magnitude peaks at these frequencies. Note that both resonant frequen-

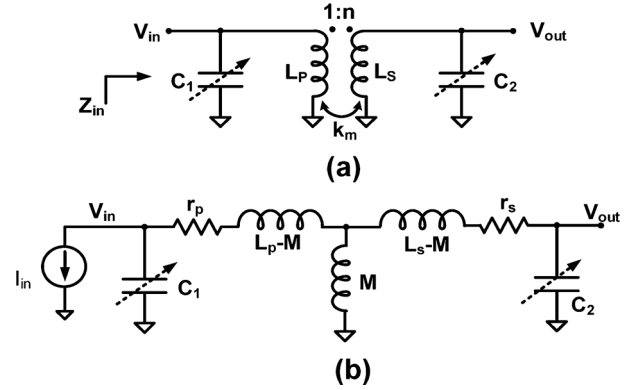


Fig. 6. Transformer-based resonator (a); and its equivalent circuit (b).

cies can satisfy the Barkhausen criterion with a sufficient loop gain [16]. However, the resulting multi-oscillation behavior is undesired and must be avoided [17]. In our case, it is preferred to see an oscillation at the lower resonant frequency  $\omega_1$  and the additional tank impedance at  $\omega_2$  is used to make a pseudo-square waveform across the tank. These two possible resonant frequencies can be expressed as

$$\omega_{1,2}^2 = \frac{1 + \left(\frac{L_s C_2}{L_p C_1}\right) \pm \sqrt{1 + \left(\frac{L_s C_2}{L_p C_1}\right)^2 + \left(\frac{L_s C_2}{L_p C_1}\right) (4k_m^2 - 2)}}{2L_s C_2 (1 - k_m^2)} \quad (5)$$

The following expression offers a good estimation of the main resonant frequency of the tank for  $0.5 \leq k_m \leq 1$ .

$$\omega_1^2 = \frac{1}{(L_p C_1 + L_s C_2)} \quad (6)$$

However, we are interested in the ratio of resonant frequencies as given by

$$\begin{cases} \frac{\omega_2}{\omega_1} = \sqrt{\frac{1 + X + \sqrt{1 + X^2 + X(4k_m^2 - 2)}}{1 + X - \sqrt{1 + X^2 + X(4k_m^2 - 2)}}} \\ X = \left(\frac{L_s}{L_p} \cdot \frac{C_2}{C_1}\right) \end{cases} \quad (7)$$

Equation (7) indicates the resonant frequency ratio  $\omega_2/\omega_1$  is just a function of the transformer inductance ratio  $L_s/L_p$ , tuning capacitance ratio  $C_2/C_1$ , and transformer magnetic coupling factor  $k_m$ . The relative matching of capacitors (and inductors) in today's CMOS technology is expected to be much better than 1%, while the magnetic coupling is controlled through lithography that precisely sets the physical dimensions of the transformer. Consequently, the relative position of the resonant frequencies is not sensitive to the process variation. The  $\omega_2/\omega_1$  ratio is illustrated versus  $X$ -factor for different  $k_m$  in Fig. 7. As

$$Z_{in} = \frac{s^3 (L_p L_s C_2 (1 - k_m^2)) + s^2 (C_2 (L_s r_p + L_p r_s)) + s (L_p + r_s r_p C_2) + r_p}{s^4 (L_p L_s C_1 C_2 (1 - k_m^2)) + s^3 (C_1 C_2 (L_s r_p + L_p r_s)) + s^2 (L_p C_1 + L_s C_2 + r_p r_s C_1 C_2) + s (r_p C_1 + r_s C_2) + 1} \quad (4)$$

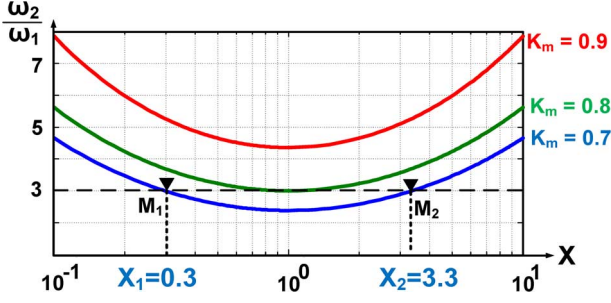


Fig. 7. Ratio of the tank resonant frequencies versus  $X$ -factor for different  $k_m$ .

expected, the ratio moves to higher values for larger  $k_m$  and finally the second resonance disappears for the perfect coupling factor. The ratio of  $\omega_2/\omega_1$  reaches the desired value of 3 at two points for the coupling factor of less than 0.8. Both points put  $\omega_2$  at the correct position of  $3\omega_1$ . However, the desired  $X$ -factor should be chosen based on the magnitude ratio  $R_{p2}/R_{p1}$  of the tank input impedance at resonance. The sum of the even orders of the denominator in (4) is zero at resonant frequencies. It can be shown that the first-order terms of the numerator and the denominator are dominant at  $\omega_1$ . By using (6), assuming  $Q_p = L_p\omega/r_p$ ,  $Q_s = L_s\omega/r_s$ , the tank input impedance at the fundamental frequency is expressed as

$$R_{p1} \approx \frac{L_p}{\omega_1 \left( \frac{L_p C_1}{Q_p} + \frac{L_s C_2}{Q_s} \right)} \xrightarrow{Q_p=Q_s=Q_0} R_{p1} \approx L_p \omega_1 Q_0 \quad (8)$$

On the other hand, it can be shown that the third-order terms of the numerator and the denominator are dominant in (4) at  $\omega_2 = 3\omega_1$ . It follows that

$$R_{p2} \approx \frac{(1 - k_m^2)}{C_1 \omega_2 \left( \frac{1}{Q_p} + \frac{1}{Q_s} \right)} \xrightarrow{Q_p=Q_s=Q_0} R_{p2} \approx \frac{Q_0 (1 - k_m^2)}{2C_1 \omega_2} \quad (9)$$

$R_{p2}$  is a strong function of the coupling factor of the transformer and thus the resulting leakage inductance. Weaker magnetic coupling will result in higher impedance magnitude at  $\omega_2$  and, consequently, the second resonance needs a lower transconductance gain to excite. It could even become a dominant pole and the circuit would oscillate at  $\omega_2$  instead of  $\omega_1$ . This phenomenon has been used to extend the oscillator tuning range in [16], [18] and [19]. As explained before,  $R_{p2}/R_{p1}$  controls the amount of the 3rd harmonic component of the oscillation voltage. The impedance magnitude ratio is equal to

$$\frac{R_{p2}}{R_{p1}} \approx \frac{(1 - k_m^2)(1 + X)}{6} \quad (10)$$

Hence, the smaller  $X$ -factor results in lower tank equivalent resistance at  $\omega_2 = 3\omega_1$ . Thus, the tank filters out more of the 3rd harmonic of the drain current and the oscillation voltage becomes more sinusoidal. Fig. 8(a) illustrates Momentum simulation results of  $Z_{in}$  of the transformer-based tank versus frequency for both  $X$ -factors that satisfy the resonant frequency

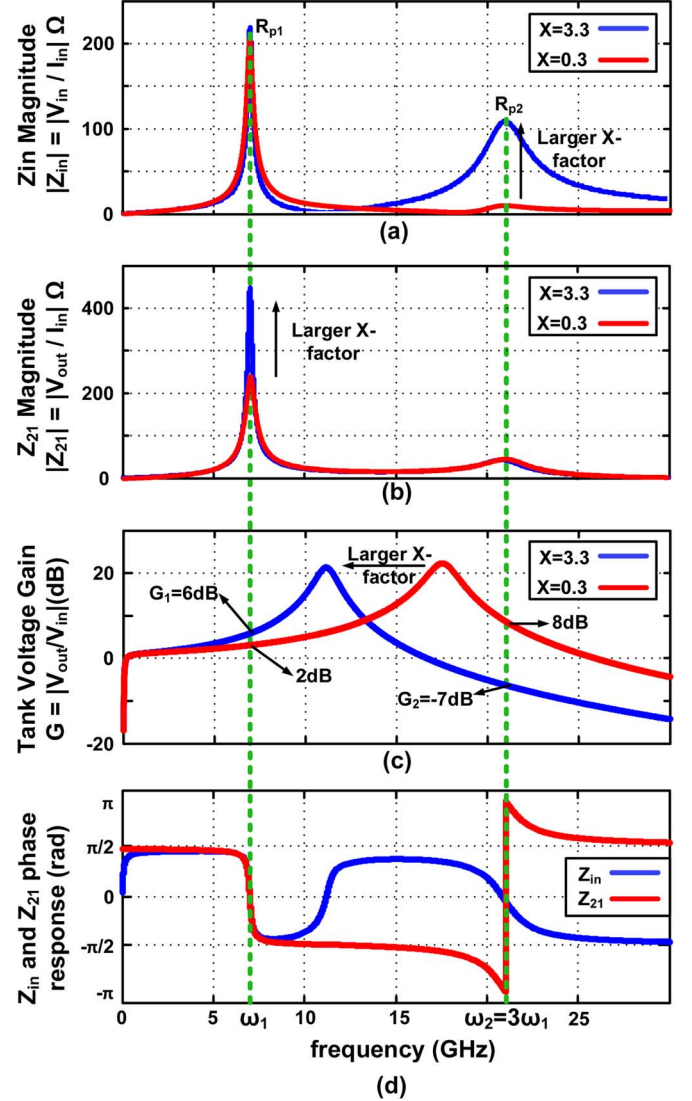


Fig. 8. The transformer-based tank characteristics: (a) the input impedance,  $Z_{in}$  magnitude; (b) the trans-impedance,  $Z_{21}$  magnitude; (c) transformer's secondary to primary voltage gain; (d) the phase of  $Z_{in}$  and  $Z_{21}$  (Momentum simulation).

ratio of 3. The larger  $X$ -factor offers significantly higher tank impedance at  $\omega_2$ , which is entirely in agreement with the theoretical analysis.

The  $X$ -factor is defined as a product of the transformer inductance ratio  $L_s/L_p$  and tuning capacitance ratio  $C_2/C_1$ . This leads to a question of how best to divide  $X$ -factor between the inductance and capacitance ratios. In general, larger  $L_s/L_p$  results in higher inter-winding voltage gain, which translates to sharper transition at zero-crossings and larger oscillation amplitude at the secondary winding. Both of these effects have a direct consequence on the phase noise improvement. However, the transformer  $Q$ -factor drops by increasing the turns ratio. In addition, very large oscillation voltage swing brings up reliability issues due to the gate-oxide breakdown. It turns out that the turns ratio of 2 can satisfy the aforementioned constraints altogether.

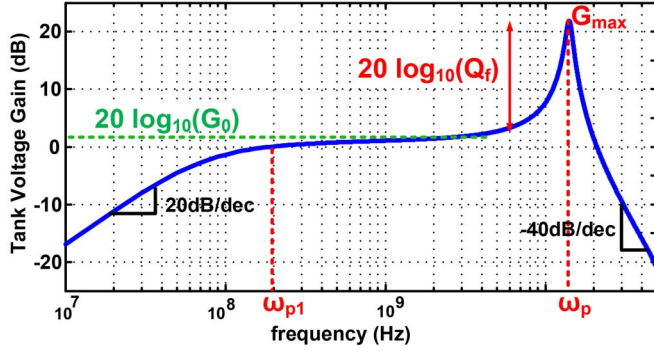


Fig. 9. Typical secondary-to-primary winding voltage gain of the transformer-based resonator versus frequency.

### C. Voltage Gain of the Tank

The transformer-based resonator, whose schematic was shown in Fig. 6, offers a filtering function on the signal path from the primary to the secondary windings. The tank voltage gain is derived in (11) shown at the bottom of the page.

Bode diagram of the tank voltage gain transfer function is shown in Fig. 9. The tank exhibits a 20 dB/dec attenuation for frequencies lower than the first pole and offers a constant voltage gain at frequencies between the first pole and the complex conjugate pole pair at  $\omega_p$ . The gain plot reveals an interesting peak at frequencies around  $\omega_p$ , beyond which the filter gain drops at the  $-40$  dB/dec slope. The low frequency pole is estimated by

$$\omega_{p1} = \frac{r_p}{L_p} \quad (12)$$

By substituting  $r_p = L_p\omega/Q_p$ ,  $r_s = L_s\omega/Q_s$  and assuming  $Q_p \cdot Q_s \gg 1$ , the tank gain transfer function can be simplified to the following equation for the frequencies beyond  $\omega_{p1}$ .

$$\begin{cases} G(s) = \frac{\frac{M}{L_p}}{s^2(L_s C_2(1 - k_m^2)) + s\left(L_s C_2 \omega \left(\frac{1}{Q_p} + \frac{1}{Q_s}\right)\right) + 1} \\ G(s) = \frac{G_0}{\left(\frac{s}{\omega_p}\right)^2 + \left(\frac{s}{\omega_p Q_f}\right) + 1} \end{cases} \quad (13)$$

The main characteristics of the tank voltage gain can be specified by considering it as a biquad filter.

$$G_0 = k_m n \quad (14)$$

The peak frequency is estimated by

$$\omega_p = \sqrt{\frac{1}{L_s C_2 (1 - k_m^2)}} \quad (15)$$

$Q_f$  represents the amount of gain jump around  $\omega_p$  and expressed by

$$Q_f = \frac{(1 - k_m^2)}{\frac{1}{Q_p} + \frac{1}{Q_s}} \quad (16)$$

Hence, the maximum voltage gain is calculated by

$$G_{\max} = k_m n \times \frac{(1 - k_m^2)}{\frac{1}{Q_p} + \frac{1}{Q_s}} \quad (17)$$

Equations (17) and Fig. 9 demonstrate that the transformer-based resonator can offer the voltage gain above  $k_m n$  at the frequencies near  $\omega_p$  for  $k_m < 1$  and the peak magnitude is increased by improving Q-factor of the transformer individual inductors. Consequently,  $\omega_1$  should be close to  $\omega_p$  to have higher passive gain at the fundamental frequency and more attenuation at its harmonic components. Equations (6) and (15) indicate that  $\omega_p$  is always located at frequencies above  $\omega_1$  and the frequency gap between them decreases with greater X-factor. Fig. 8(c) illustrates the voltage gain of the transformer-based tank for two different X-factors that exhibit the same resonant frequencies. The transformer peak gain happens at much higher frequencies for the smaller X-factor and, therefore, the gain is limited to only  $k_m n$  (2 dB in this case) at  $\omega_1$ . However, X-factor is around 3 for the proposed oscillator and, as a consequence,  $\omega_p$  moves lower and much closer to  $\omega_1$ . Now, the tank offers higher voltage gain ( $G_1 = 6$  dB in this case) at the main resonance and more attenuation ( $G_2 = -7$  dB) at  $\omega_2$ . The former translates to larger oscillation voltage swing and thus better phase noise.

As can be seen in Fig. 8(d), the input impedance  $Z_{in}$  phase is zero at the first and second resonant frequencies. Hence, any injected 3rd harmonic current has a constructive effect resulting in sharper zero-crossings and flat peak for the transformer's primary winding voltage. However, the tank trans-impedance,  $Z_{21}$  phase shows a 180 degree phase difference at  $\omega_1$  and  $\omega_2 = 3\omega_1$ . Consequently, the 3rd harmonic current injection at the primary windings leads to a slower zero-crossings slope at the transformer's secondary, which has an adverse outcome on the phase noise performance of the oscillator. Fig. 8(a)–(c) illustrates that the proposed transformer-based resonator effectively filters out the 3rd harmonic component of the drain current at the secondary winding in order to minimize these side effects and zero-crossings are sharpened by tank's voltage gain ( $G_1$ ) at  $\omega_1$ . Table I shows that the zero-crossings slope of the proposed oscillator at both transformer's windings are improved compared to the traditional oscillator for the same  $V_{DD}$ , which is translated to shorter commutating time and lower active device noise factor.

$$G(s) = \frac{V_{out}}{V_{in}} = \frac{Ms}{s^3(L_p L_s C_2(1 - k_m^2)) + s^2(C_2(L_s r_p + L_p r_s)) + s(L_p + r_s r_p C_2) + r_p} \quad (11)$$

TABLE I  
NORMALIZED ZERO-CROSSING SLOPE OF THE PROPOSED OSCILLATOR

	Normalized zero-crossing slope
Traditional LC	1
Proposed tank (primary)	$1+3\zeta = 1+3\cdot 1/6 = 1.5$
Proposed tank (secondary)	$G_1-3G_2\zeta = 2.1 - 3\cdot 0.4\cdot 1/6 = 1.9$

#### D. Proposed Class-F Oscillator

The desired tank impedance, inductance and capacitance ratios were determined above to enforce the pseudo-square-wave oscillation voltage around the tank. Now, two transistors should be customarily added to the transformer-based resonator to sustain the oscillation. There are two options, however, as shown in Fig. 10, for connecting the transformer to the active gm-devices. The first option is a transformer-coupled class-F oscillator in which the secondary winding is connected to the gate of the gm-devices. The second option is a cross-coupled class-F oscillator with a floating secondary transformer winding, which only physically connects to tuning capacitors  $C_2$ . The oscillation voltage swing, the equivalent resonator quality factor and tank input impedance are the same for both options. However, the gm-device sustains larger voltage swing in the first option. Consequently, its commutation time is shorter and the active device noise factor is lower. In addition, the gm-device generates higher amount of the 3rd harmonic, which results in sharper pseudo-square oscillation voltage with lower ISF rms value. The second major difference is about the possibility of oscillation at  $\omega_2$  instead of  $\omega_1$ . The root-locus plot in Fig. 11 illustrates the route of pole movements towards zeros for different values of the oscillator loop trans-conductance gain ( $G_m$ ). As can be seen in Fig. 11(b), both resonant frequencies ( $\omega_1, \omega_2$ ) can be excited simultaneously with a relatively high value of  $G_m$  for the cross-coupled class-F oscillator of Fig. 10(b). It can increase the likelihood of the undesired oscillation at  $\omega_2$ . However, the transformer-coupled circuit of Fig. 10(a) demonstrates a different behavior. The lower frequency conjugate pole pair moves into the right-hand plane by increasing the absolute value of  $G_m$ , while the higher poles are pushed far away from imaginary axis (see Fig. 11(a)). This guarantees the oscillation can only happen at  $\omega_1$ . Consequently, it becomes clear that the transformer-coupled oscillator is a better option due to its phase noise performance and the guaranty of operation at the right resonant frequency. Nevertheless, the gate parasitic capacitance appears at the drain through a scaling factor of  $n^2$ , which reduces its tuning range somewhat as compared to the cross-coupled candidate.

Fig. 12 illustrates the unconventional oscillation voltage waveforms of the proposed transformer-coupled class-F oscillator. As specified in Section II.C, the 3rd harmonic component of the drain voltage attenuates at the gate and thus a sinusoidal wave is seen there. The gate-drain voltage swing goes as high as  $2.7 \cdot V_{DD}$  due to the significant voltage gain of the tank. Hence, using thick oxide gm-devices is a constraint to satisfy the time-dependent dielectric breakdown (TDDB) issue for less than 0.01% failure rate during ten years of the oscillator operation [20], [21]. The costs are larger parasitic capacitance and slightly lower frequency tuning range.

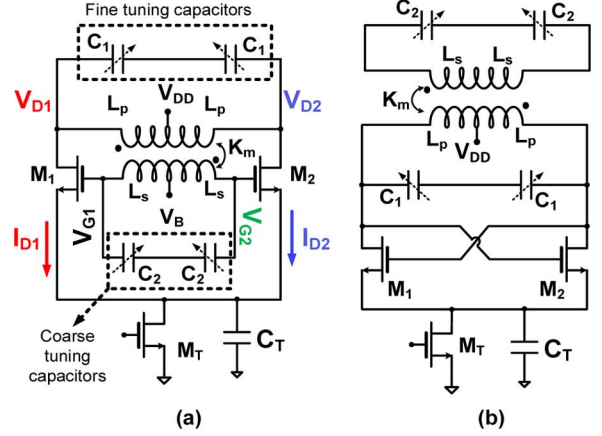


Fig. 10. Two options of the transformer-based class-F oscillator: (a) transformer-coupled; and (b) cross-coupled. The first option was chosen as more advantageous in this work.

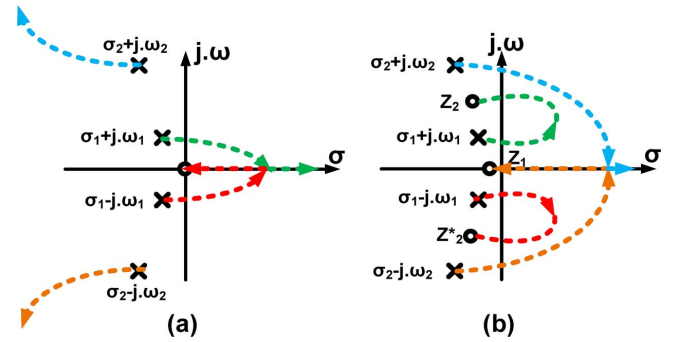


Fig. 11. Root-locus plot of the transformer-based class-F oscillator: (a) transformer-coupled structure of Fig. 10(a); and (b) cross-coupled structure of Fig. 10(b).

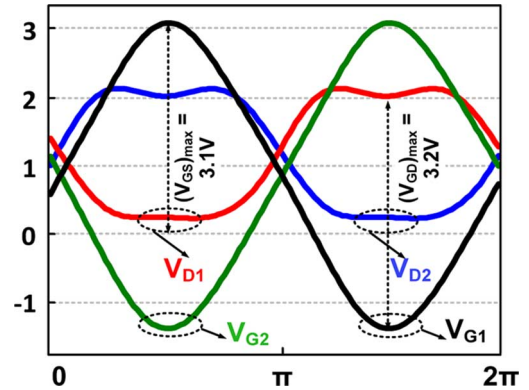


Fig. 12. Oscillation voltage waveforms of class-F oscillator.

The frequency tuning requires a bit different consideration in the class-F oscillator. Both  $C_1$  and  $C_2$  must, at a coarse level, be changed simultaneously to maintain  $L_s C_2 / L_p C_1$  ratio such that  $\omega_2$  aligns with  $3\omega_1$ .

Fig. 13 shows the transient response of the class-F oscillator. At power up, the oscillation voltage is very small and the drain current pulses have narrow and tall shape. Even though the tank has an additional impedance at  $3\omega_1$ , the 3rd harmonic component of the drain current is negligible and, consequently, the drain oscillation resembles a sinusoid. At steady state, gate oscillation voltage swing is large and the gm-device drain current is square-wave. Consequently, the combination of the tank input

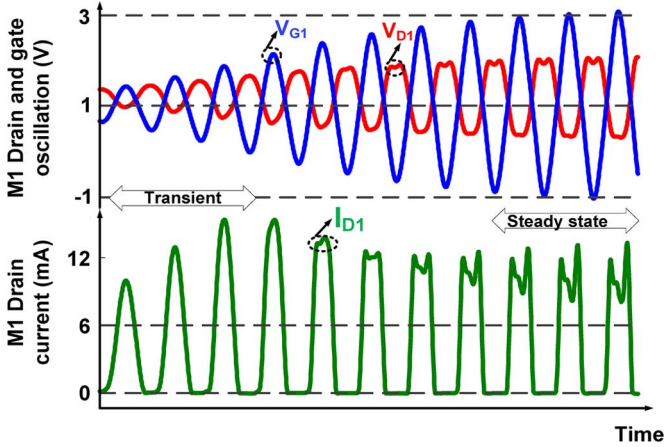


Fig. 13. Transient response of the class-F oscillator.

impedance with significant 3rd harmonic component of drain current results in the pseudo-square wave for the drain oscillation voltage. This justifies its “class-F” designation.

### III. CLASS-F PHASE NOISE PERFORMANCE

#### A. Quality Factor of Transformer-Based Resonator

The Q-factor of the complex tank, which comprises two coupled resonators, does not appear to be as straightforward in intuitive understanding as the Q-factor of the individual physical inductors. It is, therefore, imperative to understand the relationship between the open-loop Q-factor of the tank versus the Q-factor of the inductive and capacitive parts of the resonator.

First, suppose the tuning capacitance losses are negligible. Consequently, the oscillator equivalent Q-factor just includes the tank’s inductive part losses. The open-loop Q-factor of the oscillator is defined as  $\omega_0/2 \cdot d\phi/d\omega$ , where  $\omega_0$  is the resonant frequency and  $d\phi/d\omega$  denotes the slope of the phase of the oscillator open-loop transfer function [22]. To determine the open-loop Q, we need to break the oscillator loop at the gate of  $M_1$ , as shown in Fig. 14. The open-loop transfer function is thus given by

$$H(s) = \frac{V_{\text{out}}}{I_{\text{in}}} = \frac{Ms}{As^4 + Bs^3 + Cs^2 + Ds + 1} \quad (18)$$

where,  $A = (L_p L_s C_1 C_2 (1 - k_m^2))$ ,  $B = (C_1 C_2 (L_s r_p + L_p r_s))$ ,  $C = (L_p C_1 + L_s C_2 + r_p r_s C_1 C_2)$ , and  $D = (r_p C_1 + r_s C_2)$ . After carrying out lengthy algebra and considering  $(1 - C\omega^2 + A\omega^4 \approx 0)$  at the resonant frequencies,

$$Q_i = -\frac{\omega}{2} \frac{d\phi(\omega)}{d\omega} = \frac{(C\omega - 2A\omega^3)}{(D - B\omega^2)} \quad (19)$$

Substituting A, B, C and D into (19), then swapping  $r_p$  and  $r_s$  with  $L_p\omega/Q_p$  and  $L_s\omega/Q_s$ , respectively, and assuming  $Q_p Q_s \gg 1$ , we obtain

$$Q_i = \frac{(L_p C_1 + L_s C_2) - 2(L_p L_s C_1 C_2 (1 - k_m^2)) \omega^2}{\left(\frac{L_p C_1}{Q_p} + \frac{L_s C_2}{Q_s}\right) - \left(C_1 C_2 L_s L_p \left(\frac{1}{Q_p} + \frac{1}{Q_s}\right)\right) \omega^2} \quad (20)$$

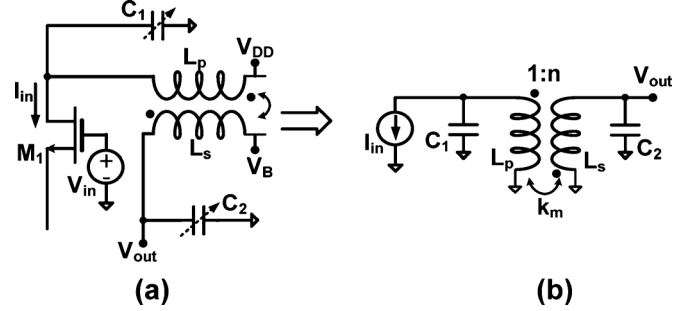


Fig. 14. Open-loop circuit for unloaded Q-factor calculation (a); its equivalent circuit (b).

Substituting (5) as  $\omega$  into the above equation and carrying out the mathematics, the tank’s inductive part Q-factor at the main resonance is

$$Q_i = \frac{(1 + X^2 + 2k_m X)}{\left(\frac{1}{Q_p} + \frac{X^2}{Q_s}\right)} \quad (21)$$

To help with an intuitive understanding, let us consider a boundary case. Suppose, that  $C_2$  is negligible. Therefore,  $X$ -factor is zero and (21) predicts that the  $Q_i$  equals to  $Q_p$ . This is not surprising, because no energy would be stored at the transformer’s secondary winding and its Q-factor would not have any contribution to the equivalent Q-factor of the tank. In addition, (21) predicts that the equivalent Q-factor of the tank’s inductive part can exceed Q-factors of the individual inductors. To the authors’ best knowledge, this is the first ever report of quantifying the equivalent Q-factor of the transformer-based resonator at its resonant frequency in a general case that clearly proves Q-factor enhancement over that of the transformer’s individual inductors. The maximum tank’s inductive part Q-factor is obtained at the following  $X$ -factor for a given  $k_m$ ,  $Q_p$  and  $Q_s$ .

$$X_{Q_{\text{max}}} = \frac{Q_s}{Q_p} \quad (22)$$

For a typical case of  $Q_s = Q_p = Q_0$ , the maximum  $Q_i$  at  $\omega_1$  is calculated by

$$\begin{cases} X_{Q_i, \text{max}} = 1 \\ Q_{i, \text{max}} = Q_0(1 + k_m) \end{cases} \quad (23)$$

The above equation indicates that the equivalent Q-factor of the inductive part of the transformer-based resonator can be enhanced by a factor of  $1 + k_m$  at the optimum state. However, it does not necessarily mean the Q-factor of the transformer-based tank generally is superior to the simple LC resonator. The reason is that it is not possible to optimize the Q-factor of both windings of a 1:n transformer at a given frequency and one needs to use lower metal layers for the transformer cross connections, which results in more losses and lower Q-factor [23], [24]. For this prototype, the  $X$ -factor is around 3 with  $k_m = 0.7$  and the simulated  $Q_p$  and  $Q_s$  are 14 and 20 respectively. Based on (21), the equivalent Q-factor of the inductive part of the tank would be about 26, which is higher than that of the transformers’ individual inductors.

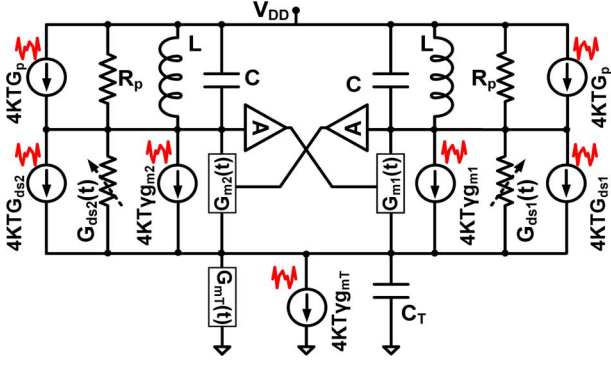


Fig. 15. RF CMOS oscillator noise sources.

The Q-factor of the switched capacitance largely depends on the tuning range (TR) and operating frequency of the oscillator and is about 42 for the TR of 25% at 7 GHz resulting in an average Q-factor of 16 for the tank in this design.

### B. Phase Noise Mechanism in Class-F Oscillator

According to the linear time-variant model [13], the phase noise of the oscillator at an offset frequency  $\Delta\omega$  from its fundamental frequency is expressed as,

$$L(\Delta\omega) = 10 \log_{10} \left( \frac{\sum_i N_{L,i}}{2q_{\max}^2 (\Delta\omega)^2} \right) \quad (24)$$

where,  $q_{\max}$  is the maximum charge displacement across the tuning capacitor C, and  $N_{L,i}$  is the effective noise produced by  $i$ th device given by

$$N_{L,i} = \frac{1}{2\pi N^2} \int_0^{2\pi} \Gamma_i^2(t) \overline{i_{n,i}^2(t)} dt \quad (25)$$

where  $\overline{i_{n,i}^2(t)}$  is the white current noise power density of the  $i$ th noise source,  $\Gamma_i$  is its relevant ISF function from the corresponding  $i$ th device noise, and  $N$  is the number of resonators in the oscillator.  $N$  is considered one for single-ended and two for differential oscillator topologies with a single LC tank [7].

Fig. 15 illustrates the major noise sources of CMOS class-B, C and F oscillators.  $R_p$  and  $G_{ds1,2}(t)$  represent the equivalent tank parallel resistance and channel conductance of the gm transistors, respectively. On the other hand,  $G_{m1,2}$  and  $G_{mT}$  model the noise due to transconductance gain of active core and current source transistors, respectively. By substituting (25) into (24) and carrying out algebra, the phase noise equation is simplified to

$$L(\Delta\omega) = 10 \log_{10} \left( \frac{K_B T R_p}{2Q_t^2 V_p^2} \cdot F \cdot \left( \frac{\omega_0}{\Delta\omega} \right)^2 \right) \quad (26)$$

where  $Q_t$  is the tank's equivalent quality factor and  $V_p$  is the maximum oscillation voltage amplitude, derived by

$$V_p = \begin{cases} \left( \frac{1}{3} + \zeta \right) \sqrt{\left( 1 + \frac{1}{3\zeta} \right)} \cdot \alpha_I \cdot R_p \cdot I_B, & \frac{1}{9} \leq \zeta \leq 1 \\ (1 - \zeta) \cdot \alpha_I \cdot R_p \cdot I_B, & 0 \leq \zeta \leq \frac{1}{9} \end{cases} \quad (27)$$

where  $\alpha_I$  is the current conversion efficiency of the oscillator, expressed as the ratio of the fundamental component of gm-devices drain current to dc current  $I_B$  of the oscillator.  $F$  in (26) is the effective noise factor of the oscillator, expressed by

$$F = \sum_i \frac{1}{2\pi} \int_0^{2\pi} \Gamma_i^2(t) \frac{\overline{i_{n,i}^2(t)} R_p}{4K_B T} dt \quad (28)$$

Suppose that  $C_T$  is large enough to filter out the thermal noise of the tail transistor. Consequently,  $F$  consists of the noise factor of the tank ( $F_{\text{tank}}$ ), transistor channel conductance ( $F_{GDS}$ ) and gm of core devices ( $F_{GM}$ ). The expressions of  $F_{\text{tank}}$  and  $F_{GDS}$  are

$$F_{\text{Tank}} = \frac{1}{\pi} \int_0^{2\pi} \Gamma_{\text{tank}}^2(t) dt = 2\Gamma_{\text{rms}}^2 \approx \frac{1 + 9\zeta^2}{(1 + 3\zeta)^2} \quad (29)$$

$$F_{GDS} = \frac{1}{\pi} \int_0^{2\pi} \Gamma_{\text{MOS}}^2(t) G_{DS1}(t) R_p dt \approx 2\Gamma_{\text{rms}}^2 R_p \cdot G_{DS1EF} \quad (30)$$

where  $G_{DS1EF}$  is the effective drain-source conductance of one of the gm-devices expressed by

$$G_{DS1EF} = G_{DS1}[0] - G_{DS1}[2] \quad (31)$$

where  $G_{DS1}[k]$  describes the  $k$ th Fourier coefficient of the instantaneous conductance,  $G_{ds1}(t)$  [25].  $F_{GM}$  can be calculated by

$$F_{GM} = \frac{1}{\pi} \int_0^{2\pi} \Gamma_{\text{MOS}}^2(t) \gamma G_{m1}(t) R_p dt \approx 2\Gamma_{\text{rms}}^2 \cdot \gamma \cdot R_p \cdot G_{M1EF} \quad (32)$$

Now, the effective negative transconductance of the oscillator needs to overcome the tank and its own channel resistance losses and therefore the noise due to  $G_M$  also increases.

$$G_{M1EF} = \frac{1}{A} \left( \frac{1}{R_p} + G_{DS1EF} \right) \quad (33)$$

where  $A$  is the voltage gain of feedback path between the tank and MOS gate. By substituting (33) into (32)

$$F_{GM} = 2\Gamma_{\text{rms}}^2 \cdot \frac{\gamma}{A} \cdot (1 + R_p G_{DS1EF}) \quad (34)$$

Consequently, the effective noise factor of the oscillator is given by

$$F = 2\Gamma_{\text{rms}}^2 \cdot \left( 1 + \frac{\gamma}{A} \right) \cdot (1 + R_p G_{DS1EF}) \quad (35)$$

This is a general result and applicable to the class-B, C and F. The oscillator FoM normalizes the phase noise performance to the oscillation frequency and power consumption, yielding

$$FoM = -10 \log_{10} \left( \frac{10^3 K_B T}{2Q_t^2 \alpha_I \alpha_V} 2\Gamma_{\text{rms}}^2 \times \left( 1 + \frac{\gamma}{A} \right) (1 + R_p G_{DS1EF}) \right) \quad (36)$$

where  $\alpha_V$  is the voltage efficiency, defined as  $V_p/V_{DD}$ . To get a better insight, the circuit-to-phase noise mechanism, relative phase noise and power efficiency of different oscillator

TABLE II  
COMPARISON OF DIFFERENT OSCILLATOR'S CLASSES FOR THE SAME  $V_{DD}$  (1.2 V), TANK Q-FACTOR (15),  $R_P$  (I.E., 220  $\Omega$ ), AND CARRIER FREQUENCY (7 GHz) AT 3 MHz OFFSET FREQUENCY

	Theoretical expression	Class-B	Dynamic biased Class-C	Class-F
$F_{RP}$	$2\Gamma_{rms}^2 = \frac{1+9\zeta^2}{(1+3\zeta)^2}$	1 (average)	1 (average)	0.7 (best)
$F_{GDS}$	$2\Gamma_{rms}^2 R_P G_{DS1EF1}$	0.56 (worst)	0.07 (best)	0.27 (average)
$F_{GM}$	$2\Gamma_{rms}^2 \frac{\gamma}{A} (1 + R_P G_{DS1EF})$	$1.56\gamma = 2.02$ (worst)	$1.07\gamma = 1.39$ (average)	$0.7\gamma = 0.91$ (best)
F (dB)	$10 \log_{10} (2 \Gamma_{rms}^2 \frac{\gamma}{A} (1 + \frac{\gamma}{A}) (1 + R_P G_{DS1EF}))$	5.5 (worst)	3.9 (average)	2.8 (best)
$\alpha_I$	$I_{H1}/I_B$	0.55 (worst)	0.9 (best)	0.63 (average)
$\alpha_V$	$V_p/V_{DD}$	0.8 (best)	0.7 (average)	0.8 (best)
PN (dBc/Hz)	$10 \log_{10} \left( \frac{K_B T R_P}{2 Q_0^2 V_p^2} \cdot F \cdot \left( \frac{\omega_0}{\Delta\omega} \right)^2 \right)$	-133.5 (worst)	-134 (average)	-136 (best)
FoM (dB)	$-10 \log_{10} \left( \frac{10^3 K_B T}{2 Q_0^2 \alpha_I \alpha_V} 2\Gamma_{rms}^2 \frac{\gamma}{A} (1 + \frac{\gamma}{A}) (1 + R_P G_{DS1EF}) \right)$	191.2 (worst)	194.5 (best)	194.2 ( $\approx$ best)

classes are also investigated and compared together in this section. Fig. 16(a)-(f) shows the oscillation voltage and drain current for the traditional, class-C and the proposed class-F oscillators for the same  $V_{DD}$  (i.e., 1.2 V), tank Q-factor (i.e., 15) and  $R_P$  (i.e., 220  $\Omega$ ).

The  $\alpha_V$  must be around 0.8 for the class B and F oscillators due to the voltage drop  $V_{dsat}$  across tail transistor needed to keep it in saturation. The combination of the tail capacitance and entering the gm-devices into the linear region reduces  $\alpha_I$  of class-B from the theoretical value of  $2/\pi$  to around 0.55. Fortunately,  $\alpha_I$  is maintained around  $2/\pi$  for class-F due to the pseudo-square drain voltage and larger gate amplitude. The class-C oscillator with a dynamic bias of the active transistor offers significant improvements over the traditional class-C, and maximizes the oscillation amplitude without compromising the robustness of the oscillator start-up [26]. Nevertheless, its  $\alpha_V$  is around 0.7 to avoid gm-devices entering the triode region. Class-C drain current composed of tall and narrow pulses results in  $\alpha_I$  equal to 0.9 (ideally 1).

Obtaining the ISF function is the first step in the calculation of the oscillator's effective noise factor. The class-B/C ISF function is a sinusoid in quadrature with the tank voltage [7], [27]. However, finding the exact equation of class-F ISF is not possible, hence, we had to resort to painstakingly long Cadence<sup>TM</sup> simulations to obtain the ISF curves. Fig. 16(g) shows the simulated class-F tank equivalent ISF function, which is smaller than the other classes for almost the entire oscillation period.

Fig. 16(h) demonstrates the tank effective noise factor along the oscillation period for different oscillator classes. The  $F_{RP}$  is 32% lower for the proposed class-F due to its special ISF properties. The gm-device  $M_1$  channel conductance across the oscillation period is shown in Fig. 16(i). As expected,  $G_{DS1}(t)$  of class-F exhibits the largest peak due to high oscillation swing at the gate and, consequently, injects more noise than other structures to the tank. On the other hand, class-C operates only in the saturation region and its effective transistor conductance is negligible. Fig. 16(j) stronger emphasizes that the gm-device resistive channel noise could even be 7 times higher than the tank noise when the  $M_1$  operates in the linear region. To get a better insight, one need to simultaneously focus on Figs. 16(j) and (k). Although the class-F  $G_{DS1}$  generates lots of noise in the second half of the period, its relevant ISF value is very small there. Hence, the excessive transistor channel noise cannot convert to the phase noise and as shown in Fig. 16(l), the  $F_{GDS}$  of class-F is one half of the traditional oscillator. The transconductance loop gain of the different oscillator structures

are shown in Fig. 16(m). Class-F needs to exhibit the highest effective transconductance loop gain to compensate its larger gm-devices channel resistance losses. However, half of the required loop gain is covered by the transformer-based tank voltage gain. Fig. 16(o) demonstrates the active device effective noise factor along the oscillation period. Class-F offers the lowest  $F_{GM}$  due to its special ISF nature and the passive voltage gain between the tank and gate of the gm-transistors.

Table II summarizes the performance of different oscillator classes of this example. It can be concluded that class-F oscillator achieves the lowest circuit-to-phase noise conversion along the best phase noise performance with almost the same power efficiency as the class-C oscillator.

The use of transformer in the Class-F configuration offers an additional reduction of the  $1/f^3$  phase noise corner. The transformer inherently rejects the common-mode signals. Hence, the  $1/f$  noise of the tail current source can appear at the transformer's primary but it will be effectively filtered out on the path to the secondary winding. Consequently, the AM-to-PM conversion at the  $C_2$  switched capacitors is entirely avoided.

Another  $1/f$  noise upconversion mechanism is called the Groszkowski effect [28]. Groszkowski demonstrated that the presence of harmonic components of the active device current in the tank can cause a frequency drift from the tank resonance [29]. The harmonic components of the drain current mainly take the capacitance path due its lower impedance. As a consequence, the oscillation frequency must shift down to satisfy the resonance condition. Consequently, any variation in harmonic-to-fundamental drain current value due to the  $1/f$  noise of  $M_T$  can modulate Groszkowski's frequency shift and show itself as a low frequency noise in the phase noise sidebands [29]. The class-F tank has fortunately two impedance peaks at the fundamental oscillation frequency and its 3rd harmonic. Hence, the 3rd harmonic component (i.e., the strongest among the higher harmonics) of drain current flows to the resistive part of the tank and does not contribute to Groszkowski's frequency shift. It effectively reduces the  $1/f$  noise upconversion to the  $1/f^3$  phase noise due to Groszkowski phenomenon.

### C. Class-F Operation Robustness

Fig. 17(a) illustrates the tank input impedance magnitude and phase for the imperfect position of the second resonance frequency  $\omega_2$ . A 6% mismatch is applied to the  $C_2/C_1$  ratio, which shifts  $\omega_2$  to frequencies higher than  $3\omega_1$ . Hence, the 3rd harmonic of the drain current is multiplied by a lower impedance

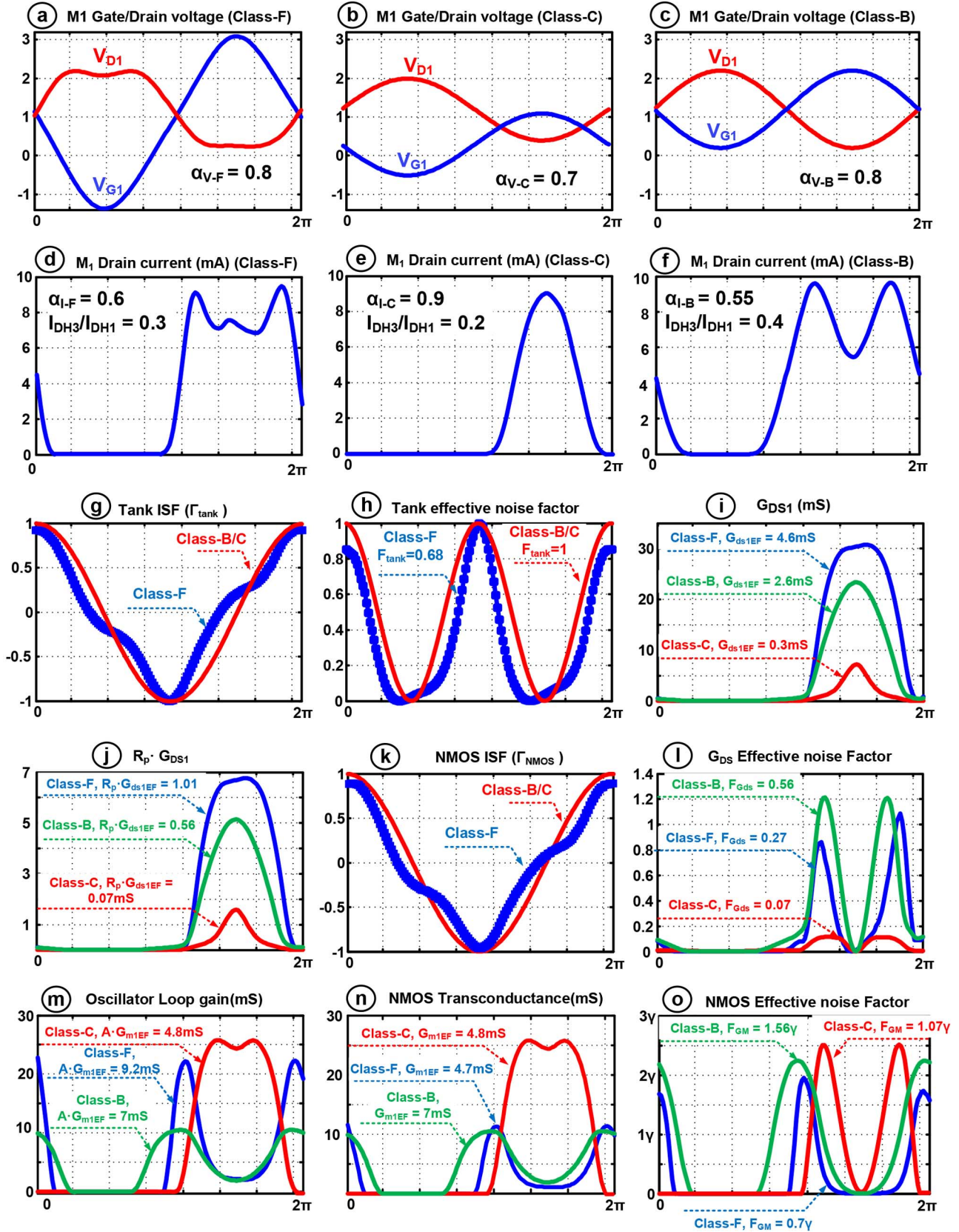


Fig. 16. Mechanisms of circuit noise to phase noise conversion in different classes of RF CMOS oscillator.

magnitude with a phase shift resulting in a distorted pseudo-square oscillation waveform as shown in Fig. 17(b). Intuitively, if the Q-factor at  $\omega_2$  was smaller, the tank impedance bandwidth around it would be wider. Therefore, the tank input impedance

phase shift and magnitude reduction would be less for a given  $\omega_2$  drift from  $3\omega_1$ . As a consequence, the oscillator would be less sensitive to the position of  $\omega_2$  and thus the tuning capacitance ratio. Based on the open-loop Q-factor analysis, substi-

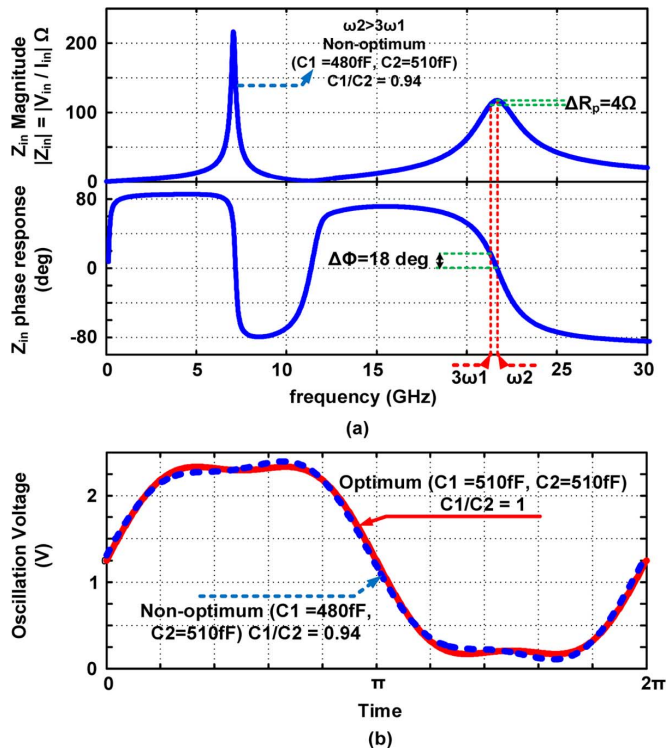


Fig. 17. Sensitivity of class-F oscillator to the position of the second resonant frequency: tank's input impedance magnitude and phase (top), oscillation waveform (bottom).

tuning  $\omega^2 \approx 9/(L_s C_2 + L_p C_1)$  into (20), the  $Q_i$  is obtained as  $0.3Q_0$  at  $\omega_2$ . Fortunately enough, the proposed tank configuration automatically reduces the equivalent tank Q-factor at  $\omega_2$  to 30% of the main resonance Q-factor. This is completely in line with the desire to reduce the sensitivity to the position of  $\omega_2$  in class-F. Consequently, a realistic example  $\pm 30$  fF variation in  $C_1$  from its optimum point has absolutely no major side effects on the oscillator waveform and thus its phase noise performance, as apparent from Fig. 17. It is strongly emphasized that the circuit oscillates based on  $\omega_1$  resonance and low Q-factor at  $\omega_2$  has no adverse consequence on the oscillator phase noise performance.

#### IV. EXPERIMENTAL RESULTS

##### A. Implementation Details

The class-F oscillator, whose schematic was shown in Fig. 10(a), has been realized in TSMC 1P7M 65-nm CMOS technology with Alucap layer. The differential transistors are thick-oxide devices of  $12(4\text{-}\mu\text{m}/0.28\text{-}\mu\text{m})$  dimension to withstand large gate voltage swing. However, the tail current source  $M_T$  is implemented as a thin-oxide  $500\text{-}\mu\text{m}/0.24\text{-}\mu\text{m}$  device biased in saturation. The large channel length is selected to minimize its  $1/f$  noise. Its large drain-bulk and drain-gate parasitic capacitances combined with  $C_T = 2$  pF MOM capacitor shunt the  $M_T$  thermal noise to ground. The step-up 1:2 transformer is realized by stacking the  $1.45\text{ }\mu\text{m}$  Alucap layer on top of the  $3.4\text{ }\mu\text{m}$  thick top (M7 layer) copper metal. Its primary and secondary differential self-inductances are about 500 pH and 1500 pH, respectively, with the magnetic coupling

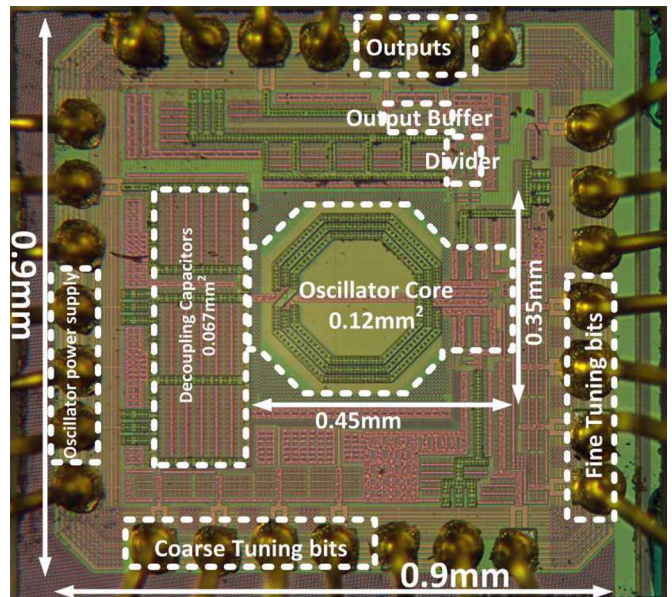


Fig. 18. Die photograph of class-F oscillator.

factor of 0.73. The transformer was designed with a goal of maximizing Q-factor of the secondary winding,  $Q_s$ , at the desired operating frequency. Based on (21),  $Q_s$  is the dominant factor in the tank equivalent Q-factor expression, provided  $(L_s C_2)/(L_p C_1)$  is larger than one, which is valid for this oscillator prototype. In addition, the oscillation voltage is sinusoidal across the secondary winding. It means the oscillator phase noise is more sensitive to the circuit noise at the secondary winding compared to the primary side with the pseudo-square waveform. Four switched MOM capacitors  $B_{C0} - B_{C3}$  placed across the secondary winding realize coarse tuning bits, while the fine control bits  $B_{F0} - B_{F3}$  with LSB size of 20 fF adjust the position of  $\omega_2$  near  $3\omega_1$ . The center tap of the secondary winding is connected to the bias voltage, which is fixed around 1 V to guarantee safe oscillator start-up in all process corners. A resistive shunt buffer interfaces the oscillator output to the dynamic divider [2]. A differential output buffer drives a 50- $\Omega$  load. The separation of the oscillator core and divider/output buffer voltage supplies and grounds serves to maximize the isolation between the circuit blocks. The die micrograph is shown in Fig. 18. The oscillator core die area is  $0.12\text{ mm}^2$ .

##### B. Measurement Results

The measured phase noise at 3.7 GHz (after the on-chip  $\div 2$  divider) at 1.25 V and 12 mA current consumption is shown in Fig. 19. The phase noise of  $-142.2$  dBc/Hz at 3 MHz offset lies on the 20 dB/dec slope, which extrapolates to  $-158.7$  dBc/Hz at 20 MHz offset ( $-170.8$  dBc/Hz when normalized to 915 MHz) and meets the GSM TX mobile station (MS) specification with a very wide 8 dB margin. The oscillation purity of the class-F oscillator is good enough to compare its performance to cellular basestation (BTS) phase noise requirements. The GSM/DCS "Micro" BTS phase noise requirements are easily met. However, the phase noise would be off by 3 dB for the toughest DCS-1800 "Normal" BTS specification at 800 kHz offset frequency [30]. The  $1/f^3$  phase noise corner is around 700 kHz at

TABLE III  
COMPARISON OF STATE-OF-THE-ART OSCILLATORS

	This Work	[9]	[8]	[30]	[10]	[31]	[2]	[19]
Technology	65nm	130nm	350 $\mu$ m	65nm	55nm	BiCMOS 130nm	90nm	65nm
Supply voltage (V)	1.25	1	2.5	1.2	1.5	3.3	1.4	0.6
Frequency (GHz)	3.7	5.2	1.2	3.92	3.35	1.56	0.915	3.7
Tuning range (%)	25	14	18	10.2	31.4	9.6	24.3	77
Phase noise at 3 MHz (dBc/Hz)	-142.2	-141.2	-152	-141.7	-142	-150.4	-149	-137.1
Norm. phase noise <sup>1</sup> (dBc/Hz)	-154.3	-147.5	-154.8	-154.4	-153.3	-155	-149	-149.21
Power consumption (mW)	15	1.4	9.25	25.2	27	290	25.2	10.5
FoM (dB)	192.2	195	195	189.9	189	180	184.6	188.7
$FoM_T^2$ (dB)	200.2	198.4	200.7	190	199	179.7	192.3	206.5
Number of inductors & transformers	1	1	2	2	1	1	1	1
Oscillator structure	Class F	Class C	Noise Filtering	Clip-and-Restore	Class B/C	Colpitts	Traditional	Dual mode

<sup>1</sup> phase noise at 3 MHz offset frequency normalized to 915 MHz carrier,

<sup>2</sup>  $FoM_T = |PN| + 20 \log_{10}((f_0/\Delta f) (TR/10)) - 10 \log_{10}(P_{DC}/1mW)$

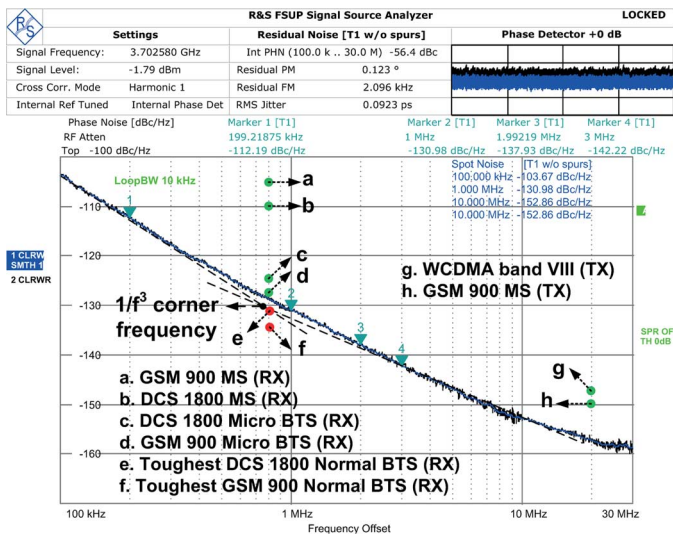


Fig. 19. Measured phase noise at 3.7 GHz and power dissipation of 15 mW. Specifications (MS: mobile station, BTS: basestation) are normalized to the carrier frequency.

the highest frequency due to the asymmetric layout of the oscillator differential nodes further magnified by the dominance of parasitics in the equivalent tank capacitance. The  $1/f^3$  phase noise corner moves to around 300 kHz at the middle and low part of the tuning range. The noise floor is  $-160$  dBc/Hz and dominated by thermal noise from the divider and buffers. The oscillator has a 25% tuning range, from 5.9 to 7.6 GHz. Fig. 20 shows the average phase noise performance of four samples at 3 MHz offset frequency across the tuning range (after the divider), together with the corresponding FoM. The average FoM is as high as 192 dBc/Hz and varies about 2 dB across the tuning range. The divided output frequency versus supply is shown in Fig. 21 and reveals very low frequency pushing of 50 MHz/V and 18 MHz/V at the highest and lowest frequencies, respectively.

The phase noise of the class-F oscillator was measured at the fixed frequency of 3.5 GHz for two configurations. In the first configuration, the  $C_2/C_1$  ratio was set to one to align the second resonant frequency  $\omega_2$  exactly at the 3rd harmonic of the fundamental frequency  $\omega_1$ . This is the optimum configuration of the class-F oscillator (Fig. 22, top). In the second con-

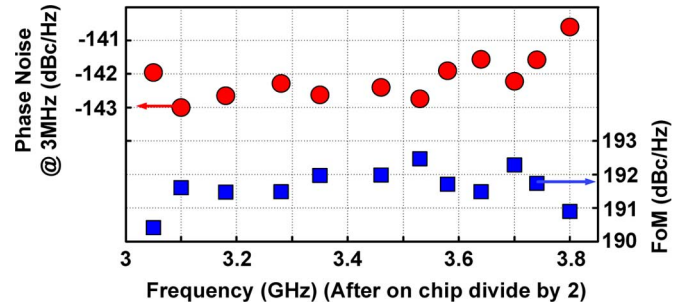


Fig. 20. Phase noise and figure-of-merit (FoM) at 3 MHz offset versus carrier frequency.

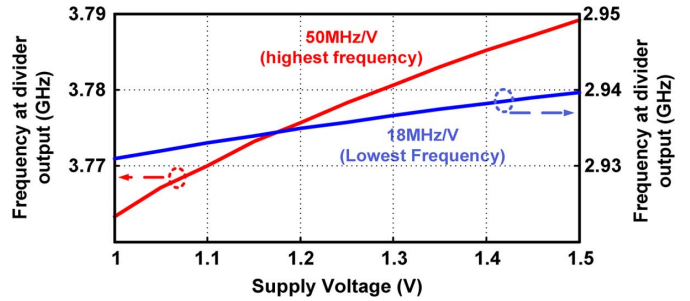


Fig. 21. Frequency pushing due to supply voltage variation.

figuration, the oscillation frequency is kept fixed but an unrealistically high 40% mismatch was applied to the  $C_2/C_1$  ratio, which lowers  $\omega_2$ , in order to see its effects on the phase noise performance (see Fig. 22, bottom). As a consequence, the 3rd harmonic component of the drain oscillation voltage is reduced and a phase shift can be seen between voltage waveform components at  $3\omega_1$  and  $\omega_1$ . Therefore, its ISF rms value is worse than optimum, thus causing a 2 dB phase noise degradation in the 20 dB/dec region. In addition, the voltage waveform demonstrates more asymmetry in the rise and fall times, which translates to the non-zero ISF dc value and increases the upconversion factor of the  $1/f^3$  phase noise corner of gm-devices. As can be seen in Fig. 22, the  $1/f^3$  phase noise corner is increased by 25% or 100 kHz in the non-optimum case. It results in a 3 dB phase noise penalty in the flicker noise region.

Table III summarizes performance of the proposed class-F oscillator and compares it with the relevant state-of-the-art. The

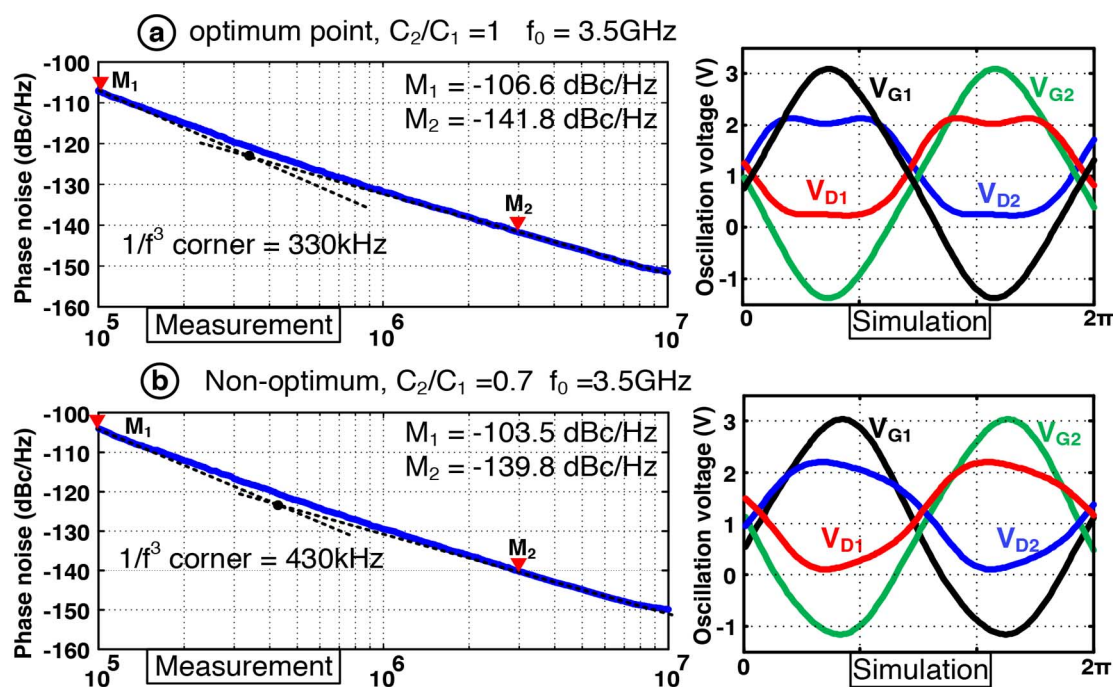


Fig. 22. Measured phase noise at 3.5 GHz and simulated oscillation waveforms: (a) optimum case; (b) exaggerated non-optimum case.

class-F demonstrates a 5 dB phase noise and 7 dB FoM improvements over the traditional commercial oscillator [2] with almost the same tuning range. For the same phase noise performance range ( $-154$  to  $-155$  dBc/Hz) at 3 MHz offset for the normalized 915 MHz carrier, the class-F oscillator consumes only 15 mW, which is much lower than with Colpitts [31], class B/C [10], and clip-and-restore [30] topologies. Only the noise-filtering-technique oscillator [8] offers a better power efficiency but at the cost of an extra dedicated inductor and thus larger die. Also, it uses a 2.5 V supply thus making it unrealistic in today's scaled CMOS. From the FoM point of view, the class-C oscillator [9] exhibits a better performance than the class-F oscillator. However, the voltage swing constraint in class-C limits its phase noise performance. As can be seen, the class-F demonstrates more than 6 dB better phase noise with almost the same supply voltage. Consequently, the class-F oscillator has reached the best phase noise performance with the highest power efficiency at low voltage supply without the die area penalty of the noise-filtering technique or voltage swing constraint of the class-C VCOs.

## V. CONCLUSION

We have proposed a new structure for LC-tank oscillators that introduces an impedance peak around the third harmonic of the oscillating waveform such that the third harmonic of the active device current converts into voltage and, together with the fundamental component, creates a pseudo-square oscillation voltage. The additional peak of the tank impedance is realized with a transformer-based resonator. As a result, the oscillator impulse sensitivity function reduces thus lowering the conversion sensitivity of phase noise to various noise sources, whose mechanisms are analyzed in depth. Chief of these mechanisms arises when the active gm-devices periodically enter the triode

region during which the LC-tank is heavily loaded while its equivalent quality factor is significantly reduced. The voltage gain, relative pole position, impedance magnitude and equivalent quality factor of the transformer-based resonator are quantified at its two resonant frequencies. The gained insight reveals that the secondary to the primary voltage gain of the transformer can be even larger than its turns ratio. A comprehensive study of circuit-to-phase-noise conversion mechanisms of different oscillators' structures shows the proposed class-F exhibits the lowest phase noise at the same tank's quality factor and supply voltage. Based on this analysis, a class-F oscillator was prototyped in 65-nm CMOS technology. The measurement results prove that the proposed oscillator can achieve a state-of-the-art phase noise performance with the highest power efficiency at low voltage power supply without die area penalty or voltage swing constraint.

## ACKNOWLEDGMENT

The authors thank A. Akhnouk, W. Straver, A. Kaichouhi, Morteza Alavi, Wanghua Wu, A. Visweswaran, A. Ahmadi Mehr, M. Tohidian, and I. Madadi for the measurement support and technical discussions.

## REFERENCES

- [1] E. Hegazi and A. A. Abidi, "A 17-mW transmitter and frequency synthesizer for 900-MHz GSM fully integrated in 0.35- $\mu$ m CMOS," *IEEE J. Solid-State Circuits*, vol. 38, no. 5, pp. 782–792, May 2003.
- [2] R. B. Staszewski *et al.*, "All-digital PLL and transmitter for mobile phones," *IEEE J. Solid-State Circuits*, vol. 40, no. 12, pp. 2469–2482, Dec. 2005.
- [3] L. Vercesi, L. Fanori, F. D. Bernardinis, A. Liscidini, and R. Castello, "A dither-less all digital PLL for cellular transmitters," *IEEE J. Solid-State Circuits*, vol. 47, no. 8, pp. 1908–1920, Aug. 2012.
- [4] H. Darabi *et al.*, "A quad-band GSM/GPRS/EDGE SoC in 65 nm CMOS," *IEEE J. Solid-State Circuits*, vol. 46, no. 4, pp. 870–882, Apr. 2011.

- [5] J. Borremans *et al.*, "A 40 nm CMOS 0.4–6 GHz receiver resilient to out-of-band blockers," *IEEE J. Solid-State Circuits*, vol. 46, no. 7, pp. 1659–1671, Jul. 2011.
- [6] J. Rael and A. Abidi, "Physical processes of phase noise in differential LC oscillators," in *Proc. IEEE Custom Integr. Circuits Conf.*, Sep. 2000, pp. 569–572.
- [7] P. Andreani, X. Wang, L. Vandi, and A. Fard, "A study of phase noise in Colpitts and LC-tank CMOS oscillators," *IEEE J. Solid-State Circuits*, vol. 40, no. 5, pp. 1107–1118, May 2005.
- [8] E. Hegazi, H. Sjolund, and A. A. Abidi, "A filtering technique to lower LC oscillator phase noise," *IEEE J. Solid-State Circuits*, vol. 36, no. 12, pp. 1921–1930, Dec. 2001.
- [9] A. Mazzanti and P. Andreani, "Class-C harmonic CMOS VCOs, with a general result on phase noise," *IEEE J. Solid-State Circuits*, vol. 43, no. 12, pp. 2716–2729, Dec. 2008.
- [10] L. Fanori, A. Liscidini, and P. Andreani, "A 6.7-to-9.2 GHz 55 nm CMOS hybrid class-B/class-C cellular TX VCO," in *IEEE Int. Solid-State Circuits Conf. (ISSCC) Dig. Tech. Papers*, Feb. 2012, pp. 354–355.
- [11] H. Kim, S. Ryu, Y. Chung, J. Choi, and B. Kim, "A low phase-noise CMOS VCO with harmonic tuned LC tank," *IEEE Trans. Microw. Theory Tech.*, vol. 54, no. 7, pp. 2917–2923, Jul. 2006.
- [12] M. Babaie and R. B. Staszewski, "Third-harmonic injection technique applied to a 5.87–to-7.56 GHz 65 nm class-F oscillator with 192 dBc/Hz FoM," in *IEEE Int. Solid-State Circuits Conf. (ISSCC) Dig. Tech. Papers*, Feb. 2013, pp. 348–349.
- [13] A. Hajimiri and T. H. Lee, "A general theory of phase noise in electrical oscillators," *IEEE J. Solid-State Circuits*, vol. 33, no. 2, pp. 179–194, Feb. 1998.
- [14] B. Razavi, "A millimeter-wave circuit technique," *IEEE J. Solid-State Circuits*, vol. 43, no. 9, pp. 2090–2098, Sep. 2008.
- [15] J. R. Long, "Monolithic transformers for silicon RF IC design," *IEEE J. Solid-State Circuits*, vol. 35, no. 9, pp. 1368–1382, Sep. 2000.
- [16] A. Bevilacqua, F. P. Pavan, C. Sandner, A. Gerosa, and A. Neviani, "Transformer-based dual-mode voltage-controlled oscillators," *IEEE Trans. Circuits Syst. II, Exp. Briefs*, vol. 54, no. 4, pp. 293–297, Apr. 2007.
- [17] A. Goel and H. Hashemi, "Frequency switching in dual-resonance oscillators," *IEEE J. Solid-State Circuits*, vol. 42, no. 3, pp. 571–582, Mar. 2007.
- [18] B. Razavi, "Cognitive radio design challenges and techniques," *IEEE J. Solid-State Circuits*, vol. 45, no. 8, pp. 1542–1553, Aug. 2010.
- [19] G. Li, L. Liu, Y. Tang, and E. Afshari, "A low-phase-noise wide-tuning-range oscillator based on resonant mode switching," *IEEE J. Solid-State Circuits*, vol. 47, no. 6, pp. 1295–1308, Jun. 2012.
- [20] R. Degraeve *et al.*, "A new model for the field dependence of intrinsic and extrinsic time-dependent dielectric breakdown," *IEEE Trans. Electron Devices*, vol. 45, no. 2, pp. 472–481, Feb. 1998.
- [21] M. Babaie and R. B. Staszewski, "A study of RF oscillator reliability in nanoscale CMOS," in *Proc. IEEE 21st European Conf. Circuit Theory and Design (ECCTD)*, Sep. 2013.
- [22] B. Razavi, "A study of phase noise in CMOS oscillators," *IEEE J. Solid-State Circuits*, vol. 31, no. 3, pp. 331–343, Mar. 1996.
- [23] H. Krishnaswamy and H. Hashemi, "Inductor and transformer-based integrated RF oscillators: A comparative study," in *Proc. IEEE Custom Integr. Circuits Conf.*, Sep. 2006, pp. 381–384.
- [24] P. Andreani and J. R. Long, "Misconception regarding of transformer resonators in monolithic oscillator," *Electronic Lett.*, vol. 42, no. 7, Mar. 2006.
- [25] D. Murphy, J. J. Rael, and A. A. Abidi, "Phase noise in LC oscillators: A phasor-based analysis of a general result and of loaded," *IEEE Trans. Circuits Syst. I, Reg. Papers*, vol. 57, no. 6, pp. 1187–1203, Jun. 2010.
- [26] L. Fanori and P. Andreani, "Low-phase-noise 3.4–4.5 GHz dynamic bias class-C CMOS VCOs with a FoM of 191 dBc/Hz," in *Proc. Eur. Solid State Circuits Conf.*, Sep. 2012, pp. 406–409.
- [27] P. Andreani and A. Fard, "More on the phase noise performance of CMOS differential-pair LC-tank oscillators," *IEEE J. Solid-State Circuits*, vol. 41, no. 12, pp. 2703–2712, Dec. 2006.
- [28] J. Groszkowski, "The impedance of frequency variation and harmonic content, and the problem of constant-frequency oscillator," *Proc. IRE*, vol. 21, pp. 958–981, 1933.
- [29] A. Bevilacqua and P. Andreani, "An analysis of 1/f noise to phase noise conversion in CMOS harmonic oscillators," *IEEE Trans. Circuits Syst. I, Reg. Papers*, vol. 59, no. 5, pp. 938–945, May 2012.
- [30] A. Visweswaran, R. B. Staszewski, and J. R. Long, "A clip-and-restore technique for phase desensitization in a 1.2 V 65 nm CMOS oscillator for cellular mobile and base stations," in *IEEE Int. Solid-State Circuits Conf. (ISSCC) Dig. Tech. Papers*, Feb. 2012, pp. 350–351.
- [31] J. Steinkamp *et al.*, "A Colpitts oscillator design for a GSM base station synthesizer," in *IEEE Radio Frequency Integrated Circuits Symp.*, Jun. 2007, pp. 405–408.



**Masoud Babaie** (S'12) received the B.Sc. degree (with highest honors) from Amirkabir University of Technology (Tehran Polytechnic), Tehran, Iran, in 2004, and the M.Sc. degree from Sharif University of Technology, Tehran, Iran, in 2006, both in electrical engineering.

He joined Kavoshcom R&D group in Tehran, Iran, in 2006 where he was involved in designing tactical communication systems. He was appointed the CTO of the company between 2009 and 2011.

He is currently working toward the Ph.D. degree at the Delft University of Technology, The Netherlands. His research interests include analog and RF IC design for wireless communications.



**Robert Bogdan Staszewski** (F'09) received the B.S.E.E. (*summa cum laude*), M.S.E.E., and Ph.D. degrees from the University of Texas at Dallas in 1991, 1992, and 2002, respectively.

From 1991 to 1995 he was with Alcatel Network Systems in Richardson, TX, USA, working on SONET cross-connect systems for fiber optics communications. He joined Texas Instruments in Dallas, TX, USA, in 1995 where he was elected Distinguished Member of Technical Staff. Between 1995 and 1999, he was engaged in advanced CMOS

read channel development for hard disk drives. In 1999, he co-started a Digital RF Processor (DRP™) group within Texas Instruments with a mission to invent new digitally intensive approaches to traditional RF functions for integrated radios in deeply-scaled CMOS processes. He was appointed a CTO of the DRP group between 2007 and 2009. In July 2009 he joined Delft University of Technology in The Netherlands, where he is a Professor. He has authored and co-authored one book, three book chapters, 150 journal and conference publications, and holds 110 issued US patents. His research interests include nanoscale CMOS architectures and circuits for frequency synthesizers, transmitters and receivers.

Prof. Staszewski has been a TPC member of ISSCC, RFIC, ESSCIRC, and RFIT. He is an IEEE Fellow and a recipient of IEEE Circuits and Systems Industrial Pioneer Award.